Solution Structure and Model Membrane Interactions of Temporins-SH, Antimicrobial Peptides from Amphibian Skin. A NMR Spectroscopy and Differential Scanning Calorimetry Study†

Feten Abbassi,‡,§ Cécile Galanth,‡ Mohamed Amiche,‡ Kazuko Saito,|| Christophe Piesse,⊥ Loussiné Zargarian,# Khaled Hani,§ Pierre Nicolas,‡ Olivier Lequin,|| and Ali Ladram*,‡

UPMC Univ Paris 06, CNRS FRE 2852, Peptidome de la Peau des Amphibiens, F-75005 Paris, France, Laboratoire de Biochimie, Faculté de Médecine de Sousse, 4002 Sousse, Tunisia, UPMC Univ Paris 06, CNRS UMR 7613, Synthèse, Structure et Fonction de Molécules Bioactives, F-75005 Paris, France, UPMC Univ Paris 06, Plate-forme Ingénierie des Protéines et Synthèse Peptidique, IFR 83, F-75005 Paris, France, and LBPA, CNRS UMR 8113, bâtiment IDA, Ecole Normale Supérieure de Cachan, 61 avenue du Président Wilson, 94235 Cachan cedex, France

Received April 18, 2008; Revised Manuscript Received July 15, 2008

ABSTRACT: Temporin-SHa and temporin-SHc are 13 residue long antimicrobial peptides from frog skin that have similar sequences but differ markedly in their membrane-damaging properties. Temporin-SHa contains a single basic lysine residue and has a unique antimicrobial spectrum of action among temporins, being very potent against Gram-positive and Gram-negative bacteria, yeasts, fungi, and protozoa. Temporin-SHc, which contains a single basic histidine residue, is inactive against Gram-negative bacteria, has a reduced efficacy against Gram-positive bacteria, but is still active against yeasts and fungi. Temporin-SHb, with no basic residue, has no antimicrobial activity. The three-dimensional structures of the peptides bound to SDS micelles were analyzed by CD and NMR spectroscopy combined with restrained molecular dynamics calculations. The peptides adopt well-defined amphipathic α-helical structures extending from residue 3 to residue 12, when bound to SDS micelles. The structures are stabilized by extensive interactions between aliphatic and aromatic side chains on the nonpolar face. Relaxation enhancements caused by paramagnetic probes showed that the peptides adopt nearly parallel orientations to the micelle surface and do not deeply penetrate into the micelle. The interaction of the peptides with model membranes was investigated by differential scanning calorimetry on anionic and zwitterionic multilamellar vesicles and membrane-permeabilization assays on calcein-loaded large unilamellar vesicles. Calorimetric data indicated that both temporin-SHa and -SHc reside at the hydrocarbon core−water interface of the anionic lipid bilayer but interact with anionic bilayers in a very different manner. This suggests that the charge-induced activity of temporins-SH for bacterial cells is due to changes in the membrane-disturbing mechanism of the bound peptides.

Temporins form a vast family of linear, highly hydrophobic and weakly charged antimicrobial peptides that are produced by the skin of Eurasian and New World ranid frogs (*1*–*4*). These peptides are of particular interest because they contain only 10−13 amino acid residues and thus are among the shortest microbicidal peptides found in nature. Temporins represent a good minimal model for membrane-destabilizing peptide with various selectivity as well as attractive templates for the design of new therapeutic agents against microbial pathogens. In most cases, there is a direct correlation between the antimicrobial potency and factors such as the length and the net positive charge of temporins. Ten-residue members of this family, although containing a basic residue, were inactive and 13-residue members carrying a net charge of 0 or +1 were inactive also (*5*). Most naturally occurring temporins contain a single basic amino acid residue (usually lysine) and show potent antimicrobial activity against Gram-positive bacteria, including clinical isolates of methicillin-resistant *Staphylococcus aureus* and vancomycin-resistant *Enterococcus faecium* and *Enterococcus faecalis* (*6, 7*), but are inactive against Gram-negative bacteria. A few temporins have also leishmanicidal activity at concentrations that are not toxic to human red blood cells (*8*). Only temporin L (FVQWFSKFLGRIL$_{amide}$) from *Rana temporaria* (*9*) and temporin-1DRa (HFLGTLVNLAKKIL$_{amide}$) from *Rana draytonii* (*10*), which bear a net charge of +3, exhibit very broad spectra of activity against Gram-positive and Gram-negative bacteria and yeasts. However, these peptides are appreciably hemolytic against human erythrocytes.

† This work was supported by grants from the Centre National de la Recherche Scientifique (CNRS). F.A. was supported by a FEBS Short-Term Fellowship and by a grant from the Tunisian Secretariat of Scientific Research.

* To whom correspondence should be addressed. Phone: +33-144275686. Fax: +33-144275994. E-mail: ali.ladram@upmc.fr.

‡ UPMC Univ Paris 06, CNRS FRE 2852, Peptidome de la Peau des Amphibiens.

§ Laboratoire de Biochimie, Faculté de Médecine de Sousse.

|| UPMC Univ Paris 06, CNRS UMR 7613, Synthèse, Structure et Fonction de Molécules Bioactives.

⊥ UPMC Univ Paris 06, Plate-forme Ingénierie des Protéines et Synthèse Peptidique.

LBPA, CNRS UMR 8113, bâtiment IDA, Ecole Normale Supérieure de Cachan.

10.1021/bi8006884 CCC: $40.75
Published on Web 09/17/2008

Table 1: Amino Acid Sequences, Net Charges, Mean Hydrophobic Moments,[a] and Hydrophobicities[a] of Temporins from *P. saharica* Skin

Peptide	Sequence[b]	Net charge (pH 7.5)	Mean Hydrophobic Moment	Mean Hydrophobicity
Temporin-SHa	**FLSGIVGMLGKLF**$_a$	+2	4.57	3.46
Temporin-SHb	**FLPIVTNLLSGLL**$_a$	+1	3.87	4.11
Temporin-SHc	**FLSHIAGFLSNLF**$_a$	+1	4.58	3.44

[a] Calculated using http://www.bbcm.univ.trieste.it/~tossi/HydroCalc/HydroMCalc.html. [b] Identical amino acid residues are in bold type; a, amide.

The detailed mechanisms by which the temporins act against microbial cells remain unclear. Experimental evidence suggests that direct peptide−lipid interactions are important for the expression of antimicrobial activity of these peptides (*4*). Temporins form amphipathic α-helices with alternating hydrophobic and polar residues in apolar media or membrane mimetic environments (*5, 6, 11*). The amphipathic α-helical structure is believed to enable the cationic peptides to interact with, and insert into the anionic outer leaflet of bacterial cytoplasmic membrane, thereby provoking membrane permeabilization and/or disruption either by their ability to form transmembrane pores via a "barrel-stave" mechanism or by a carpet on the membrane surface via a "carpet-like" model or to act as detergents via a "detergent-like" model (*5, 6, 12–14*). Since the bacterial cytoplasmic cell membrane is rich in anionic phospholipids, such as phosphatidylglycerol and negatively charged lipopolysaccharides, an increase in peptide cationicity should promote stronger interaction with the negatively charged bacterial cell membrane through nonspecific long-range Coulombic interactions and should increase antimicrobial potency. Another important question that also remains to be answered is whether the charge-induced activity of temporins for bacterial cells is due only to changes in lipid affinity or whether differences in the membrane-disturbing activity of the bound peptides are also involved.

We have recently isolated novel, 13 residue long temporins from the skin of the North African frog *Pelophylax (Rana) saharica* (*15*) that have similar sequences and hydrophobicities but differ markedly in their net charges and membrane-damaging properties (Table 1). Since a new nomenclature was recently proposed for antimicrobial peptides from the frogs of the family *Ranidae* (*16*), temporins-1S from *P. saharica* were renamed temporins-SH herein. Temporin-SHa, which contains a single lysine residue (net charge +2), is very potent against Gram-positive and Gram-negative bacteria, yeasts, and fungi (Table 2) and kills both the promastigote and the mammalian intracellular stage (amastigote) of the parasite *Leishmania infantum* without harmful effect on the macrophages (unpublished results). To our knowledge,

Table 2: Antimicrobial and Hemolytic Activity of *P. saharica* Temporins

	MIC (μM)[b]		
	temporin-SHa	temporin-SHb	temporin-SHc
Gram-positive bacteria			
S. aureus ATCC 25923	3	58	10
E. faecalis ATCC 29212	10	>116	>80
B. megaterium	2	46	4
Gram-negative bacteria			
E. coli ATCC 25922	10	231	>161
E. coli ATCC 35218	10	>116	>80
P. aeruginosa ATCC 27853	20	>231	>161
fungus			
A. flavus	ND[a]	58	10
yeasts			
C. albicans ATCC 90028	16	>116	20
C. parapsilosis ATCC 22019	31	>116	20
S. cerevisiae	8	>116	10

	LC_{50} (μM)[b]		
	temporin-SHa	temporin-SHb	temporin-SHc
erythrocytes	25	>116	>80

[a] ND, not determined. [b] MICs and LC_{50} are the average values from three independent experiments performed in triplicate.

Temp-SHa[1] is the first member of the temporin family with a net charge of +2 that exhibits a broad spectrum of antimicrobial activity. Yet, the lack of three-dimensional structural data and biophysical studies on the interaction of Temp-SHa with model membranes made it impossible to draw sound conclusions as to how this unique peptide acts on bacterial cells. In contrast, Temp-SHc, which contains a single histidine residue (net charge +1 at pH 7.5) is inactive against Gram-negative bacteria and has a reduced efficacy against Gram-positive bacteria but is still highly active against yeasts and fungi. Temp-SHb (net charge +1), which has no basic residue, has no antimicrobial activity. A comparison of the three-dimensional structures and mode of actions of these peptides, therefore, should allow one to evaluate whether 13-residue temporin family members carrying a net charge of +1 are only weakly active or inactive against bacteria because they cannot bind to anionic phospholipid membranes or, if they are bound, cannot organize themselves into structures that lyse the membrane.

We have now determined the solution structure of Temp-SHa and Temp-SHc once bound to negatively charged SDS micelles using CD and NMR spectroscopy in combination with molecular dynamics calculations. The solution structure of Temp-SHb, which has no antimicrobial activity, is also reported for comparison. SDS was used to mimic negatively charged bacterial membranes and because the small negatively charged headgroup of SDS is similar to the negatively

[1] Abbreviations: ACN, acetonitrile; CD, circular dichroism; CSD, chemical shift deviation; DMPC, dimyristoylphosphatidylcholine; DMPG, dimyristoylphosphatidylglycerol; DSC, differential scanning calorimetry; HSQC, heteronuclear single-quantum correlation; MALDI-TOF, matrix-assisted laser desorption/ionization time of flight; MIC, minimal inhibitory concentration; MLVs, multilamellar lipid vesicles; NMR, nuclear magnetic resonance; NOE, nuclear Overhauser effect; NOESY, NOE spectroscopy; RP-HPLC, reverse-phase high-performance liquid chromatography; SDS, sodium dodecyl sulfate; Temp, temporin; TFA, trifluoroacetic acid; TFE, trifluoroethanol; TOCSY, total correlation spectroscopy.

charged phosphatidic acid and phosphatidylglycerol headgroups of the plasma membrane of *Candida* species against which temporins-SH are active. In addition, the micelle size of the detergent is hardly influenced by the small size of the temporins. Furthermore, we characterized the interaction of Temp-SHa and Temp-SHc with MLVs of varying phospholipid composition by differential scanning calorimetry. Mechanisms of membrane perturbation by temporins are proposed, based on the results presented herein as well as previous findings.

EXPERIMENTAL PROCEDURES

Solid-Phase Peptide Synthesis. Fmoc-protected amino acids were purchased from Novabiochem (Switzerland), resin was from Senn Chemicals (Switzerland), and solvents were from SDS (France). Temporin-SHa, -SHb, and -SHc were synthesized using solid-phase FastMoc chemistry procedures on an Applied Biosystems 433A automated peptide synthesizer as described (*17*). The peptides were purified by RP-HPLC on a Waters RCM compact preparative cartridge module (300 Å, 25 × 100 mm) eluted at a flow rate of 8 mL/min by a 0−60% linear gradient of ACN (0.07% TFA) in 0.1% TFA/H_2O (1% ACN/min). The homogeneity and identity of the synthetic peptides were assessed by MALDI-TOF mass spectrometry (Voyager DE-PRO, Applied Biosystems) and analytical RP-HPLC on a Symmetry C-18 column (5 μm, 4.6 × 250 mm; Waters) using the conditions above with a flow rate of 0.75 mL/min.

Antimicrobial Assays. Bacteria (*Escherichia coli* ATCC 25922, *E. coli* ATCC 35218, *S. aureus* ATCC 25923, *E. faecalis* ATCC 29212, *Bacillus megaterium*, and *P. aeruginosa* ATCC 27853) were cultured in LB medium. Yeast (*Saccharomyces cerevisiae*, *Candida albicans* ATCC 90028, and *Candida parapsilosis* ATCC 22019) and fungal strains (*Aspergillus flavus*) were cultured in YPD medium. The minimal inhibitory concentration (MIC) of synthetic Temp-SHa, Temp-SHb, and Temp-SHc was determined as previously described (*18*). MIC was expressed as the lowest concentration of peptide that completely inhibited bacterial growth and as the average value from three independent experiments, each performed in triplicate with positive (0.7% formaldehyde) and negative (without peptide) inhibition control, and sterility control (H_2O). The hemolytic activity of Temp-SHa, -SHb, and -SHc was determined using fresh human erythrocytes from a healthy donor. Synthetic peptides (1−200 μM) were incubated with washed human erythrocytes (2×10^7 cells) in Dulbecco's phosphate-buffered saline, pH 7.4 (100 μL), for 1 h at 37 °C. After centrifugation (12000*g* for 15 s), the absorbance at 450 nm of the supernatant was measured. A parallel incubation in the presence of 0.1% v/v Triton was carried out to determine the absorbance associated with 100% hemolysis. The LC_{50} value corresponding to the mean concentration of peptide producing 50% hemolysis was determined from three independent experiments performed in triplicate.

CD Spectroscopy. The far-ultraviolet CD spectra were recorded at 25 °C in a Jobin-Yvon CD6 spectropolarimeter using a quartz cell of 0.1 cm path length. The instrument outputs were calibrated with *d*(+)-10-camphorsulfonic acid. Temporin-SHa, -SHb, and -SHc were solubilized in H_2O milliQ at a concentration of 10 μM with and without 40% trifluoroethanol (TFE) or 80 mM sodium dodecyl sulfate (SDS). The CD spectra were acquired between 190 and 260 nm with a spectral bandwidth of 2 nm. Each spectrum was averaged from four successive scans. The baselines (H_2O, 40% TFE, and 80 mM SDS) were acquired independently under the same conditions and then subtracted from the corresponding peptide spectra. Circular dichroism measurements are reported as $\Delta\epsilon/n$, where $\Delta\epsilon$ is the dichroic increment ($M^{-1} \cdot cm^{-1}$) and n is the number of residues in the peptide. The relative helix content was estimated according to the relation % helix $= -(\Delta\epsilon_{222\ nm} \times 10)/n$.

NMR Spectroscopy. The NMR samples were prepared in 550 μL of H_2O/D_2O (90:10 v/v) or D_2O containing 80 mM SDS-d_{25} (Eurisotop, France), using peptide concentrations of 1−2 mM. Sodium 3-(trimethylsilyl)propionate-2,2,3,3-d_4 (Isotec, Sigma Aldrich) was used as an internal reference for chemical shift calibration. The NMR experiments were recorded on a Bruker Avance III spectrometer equipped with a $^1H/^{13}C/^{15}N/^2H$ *Z*-gradient TCI cryoprobe and operating at a ^1H frequency of 500 MHz. All spectra were recorded at a temperature of 309.5 K. Two-dimensional homonuclear TOCSY and NOESY experiments were collected with 512 t_1 increments and 4096 data points in t_2, over a spectral width of 12 ppm in both dimensions. The relaxation delay was set to 1−1.2 s. A DIPSI-2 mixing sequence (*19*) was used in the TOCSY experiments with durations of 23 and 63 ms. NOESY experiments were recorded with mixing times of 50 and 150 ms. The solvent signal was suppressed by a WATERGATE sequence (*20*) and water flip-back pulses (*21, 22*). Two-dimensional $^1H-^{13}C$ HSQC spectra were recorded using gradient pulses for coherence selection (*23*). NMR experiments were processed with the Bruker TOPSPIN 2.0 program. Time-domain data were typically multiplied by shifted sine-bell functions and zero-filled prior to Fourier transformation. Indirect dimensions were extended by linear prediction. Baseline distortions were corrected with a fifth-order polynomial function. Spectra were analyzed with the aid of the XEASY program (*24*). $^3J_{HN\text{-}H\alpha}$ coupling constants were extracted with the INFIT program from F_2 rows selected on 2D NOESY spectra (*25*). $^3J_{H\alpha\text{-}H\beta}$ coupling constants were measured on F_2 rows on 2D NOESY experiments recorded in D_2O. The ^1H and ^{13}C chemical shifts of temporin-SHa, -SHb, and -SHc have been deposited in the BioMagResBank (BMRB; http://www.brmb.wisc.edu) under accession numbers 20016, 20017, and 20018, respectively. The chemical shift deviations (CSDs) of ^1H and ^{13}C resonances were calculated using a set of random coil values reported in water (*26*).

Titrations with Paramagnetic Probes. NMR samples used for the paramagnetic relaxation enhancements contained 1 mM of each temporin peptide in the presence of 80 mM deuterated SDS in H_2O/D_2O (90:10 v/v). Titrations with paramagnetic Mn^{2+} ion were performed by stepwise additions of microliter amounts of a 80 mM $MnCl_2$ solution in D_2O, to a final concentration of 0.3 mM. Assuming an average number of 60 SDS molecules per micelle, this corresponds to 0.23 Mn^{2+} ion per micelle. 5-Doxylstearic acid (Sigma Aldrich) was dissolved in CD_3OH (0.37 M) and added to the samples to obtain final concentrations of 6.7 mM (corresponding to five spin labels per micelle). The paramagnetic relaxation enhancements were monitored by recording 1D spectra after each addition of paramagnetic

agent. 2D TOCSY spectra were recorded with a mixing time of 63 ms and a relaxation delay of 4s, in the absence and in the presence of paramagnetic agents. Cross-peak volumes were integrated using the TOPSPIN program.

NMR Restraints. Interproton distance restraints were estimated from NOESY cross-peak intensities. Three upper limit classes of 2.8, 3.3, and 3.8 Å were defined depending on cross-peak intensities in the NOESY spectra recorded with a short mixing time (50 ms) to avoid spin diffusion. Additional cross-peaks observed on NOESY spectra with a longer mixing time (150 ms) were converted to upper limits of 5 Å. The ϕ torsion angle was restrained between −90° and −30° for residues exhibiting $^3J_{\text{HN-H}\alpha}$ coupling constants smaller than 6 Hz and between −170° and −70° for residues having $^3J_{\text{HN-H}\alpha}$ coupling constants larger than 8 Hz. Some χ_1 torsion angles could be restrained from the analysis of intraresidual and sequential NOEs together with $^3J_{\text{H}\alpha\text{-H}\beta}$ coupling constants.

Structure Calculation. For each peptide, a set of 50 structures was calculated by torsion angle dynamics in DYANA using standard parameters (*27*). The best 25 structures having the lowest target function were then minimized using XPLOR-NIH program (*28*) and CHARMM22 force field. Nonbond terms consisted of a Lennard-Jones potential and an electrostatic potential with a distance-dependent dielectric $\epsilon = 4r$. The 20 structures exhibiting the lowest energies were selected to represent the NMR ensemble. Structures were analyzed using InsightII (Accelrys, San Diego, CA) and PROCHECK-NMR programs (*29*). The distance restraints and NMR structures of temporin-SHa, -SHb, and -SHc have been deposited within the BioMagResBank (BMRB; http://www.brmb.wisc.edu) under accession numbers 20016, 20017, and 20018, respectively.

Differential Scanning Calorimetry. DMPC and DMPG were purchased from Avanti Polar Lipids. One milligram of phospholipids was dissolved in chloroform/methanol (1:1) (DMPG) or chloroform (DMPC). The samples were then dried under a nitrogen stream, and films were kept under vacuum for 3 h to remove all traces of organic solvents. MLVs were formed by hydrating the dry lipid film with 1 mL of PBS buffer (10 mM phosphate, 100 mM NaCl, pH 7.3) at temperatures >10 °C above the lipid phase transition and vortexing until a homogeneous suspension was formed (1 mg of MLVs/mL). Appropriate volumes of the MLV suspension (DMPG or DMPC) and Temp-SHa (1 mM) or Temp-SHc (1 mM) were mixed to obtain different desired lipid:peptide molar ratios (1:200, 1:100, and 1:50). Calorimetry experiments were performed using a Nano III calorimeter (Calorimetry Sciences Corp.). Ten scans were run for each sample, with 10 min equilibration time between each scan. Heating and cooling rates of 0.5 and 1.5 °C/min, respectively, were used over a temperature range of 0−40 °C. The raw data corresponding to the heating scans were converted to molar heat capacity, and the values for transition temperature and enthalpy were estimated using CpCalc software. For each conversion, the average lipid molecular weight for each sample and a partial specific volume of 0.730 mL/g were used.

Preparation of Calcein-Loaded Liposomes and Leakage Experiments. Dry lipid films of DMPG and DMPC (20 mg) were prepared in a similar manner to that described for DSC experiments. DMPG and DMPC LUVs with entrapped calcein were prepared by hydrating the dried lipid film with 1 mL of 10 mM Tris-HCl buffer, pH 7.4, containing 70 mM calcein. After seven rounds of freeze−thawing, the lipid suspension was extruded successively through a 400 nm polycarbonate membrane (5 times), a 200 nm polycarbonate membrane (5 times), and a 100 nm polycarbonate membrane (10 times). The average hydrodynamic diameter of the vesicles was about 100 nm, as determined by dynamic light scattering measurements using a Malvern Zetasizer Nano ZS (Malvern Instruments, Worcestershire, U.K.). Nonencapsulated calcein was removed by ultracentrifugation (100000*g*, 90 min, 4 °C), and the resulting pellet was washed twice with isosmotic buffer (10 mM Tris-HCl, 100 mM NaCl, pH 7.4). Peptide-induced leakage reflected by an increase in fluorescence was investigated by using a Perkin-Elmer luminescence spectrofluorometer (model LS50B) at excitation and emission wavelengths of 496 and 515 nm, respectively. The percent leakage values induced by various concentrations of Temp-SHa and Temp-SHc were calculated according to the equation % leakage = $[(F - F_0)/(F_{\max} - F_0)] \times 100$, where F and F_0 denote the fluorescence intensities observed with and without peptide, respectively, and $F_{\max}$ represents the fluorescence after addition of 20 μL of 10% Triton X-100 (final volume = 300 μL).

RESULTS

Antimicrobial Activity of Temporin-SHa, -SHb, and -SHc. The antimicrobial activities of synthetic Temp-SHa, -SHb, and -SHc were assayed against Gram-positive and Gram-negative bacteria, filamentous fungi, and yeasts (Table 2). Despite the paralogous relationships of the three peptides, their spectra of action differ considerably. Temp-SHa was active against most of the tested microorganisms at micromolar concentrations. The dose−response profiles showed sharp curves in which 0−100% inhibition was generated within a 1−2-fold peptide dilution. When MIC well contents (*S. aureus* and *B. megaterium*) were spread on agar plates and incubated overnight at 37 °C, no bacterial growth was observed, indicating that Temp-SHa is bactericidal. Temp-SHc was inactive against Gram-negative bacteria and *E. faecalis*. However, it effectively inhibited the proliferation of yeasts and fungi. Temp-SHb was virtually inactive against all the tested microorganisms. Tests of the peptides' hemolytic activity against human erythrocytes (Table 2) showed that Temp-SHa has moderate hemolytic activity above the MIC values observed for most of the bacterial strains tested.

Secondary Structure of Temporin-SHa, -SHb, and -SHc As Examined by CD Spectroscopy. Preliminary indications of the peptides' secondary structure were obtained by CD measurements in water, in TFE/water mixtures, and in SDS (Figure 1). The CD spectra of synthetic Temp-SHa, -SHb, and -SHc (10 μM) in aqueous solution showed that the peptides have very little ordered structure. The same peptides had helical-ordered structures with the characteristic minima at 208 and 222 nm when mixed with 40% TFE (20%, 35%, and 30% α-helix content for Temp-SHa, -SHb, and -SHc, respectively), a structure-promoting solvent, or with 80 mM SDS (39%, 41%, and 30% α-helix content for Temp-SHa, -SHb, and -SHc, respectively), a membrane-mimetic environment.

NMR Spectroscopy of Temporins in Micellar SDS. The conformations of temporins were investigated by NMR

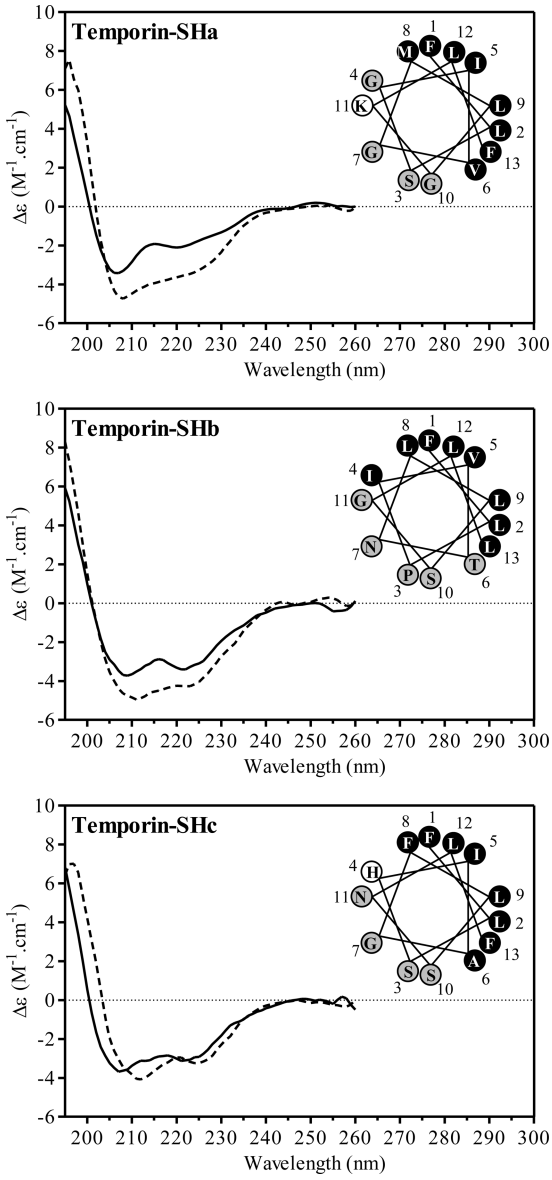

FIGURE 1: Circular dichroism spectra and helical wheel diagrams of synthetic temporin-SHa, -SHb, and -SHc. The spectra of each peptide (10 μM) were obtained in 40% TFE (solid lines) and 80 mM SDS (dotted lines). The amphipathic nature of the α-helical projections is highlighted with the hydrophobic residues indicated in black circles, the polar residues in gray circles, and the basic residues in white circles.

spectroscopy in 80 mM SDS. The NMR spectra of the three peptides exhibited good chemical shift dispersion and were suitable for structural investigation. Sequence-specific resonance assignments were obtained from the analysis of homonuclear TOCSY and NOESY experiments. Heteronuclear $^{1}H-^{13}C$ HSQC experiments were also analyzed to facilitate the side chain assignment and provide additional conformational probes through Cα and Cβ chemical shifts. The chemical shift deviations (CSDs) of ^{1}H and ^{13}C resonances, corresponding to the differences between observed chemical shifts and values obtained for the same residues in random coil state, are good indicators of structuration. For the three peptides, most residues exhibit upfield shift of their Hα resonance (average CSDs of −0.18, −0.19, and −0.20 ppm for Temp-SHa, -SHb, and -SHc, respectively) and downfield shift of their Cα resonance (average CSDs of 2.1, 2.2, and 2.3 ppm), indicating that they

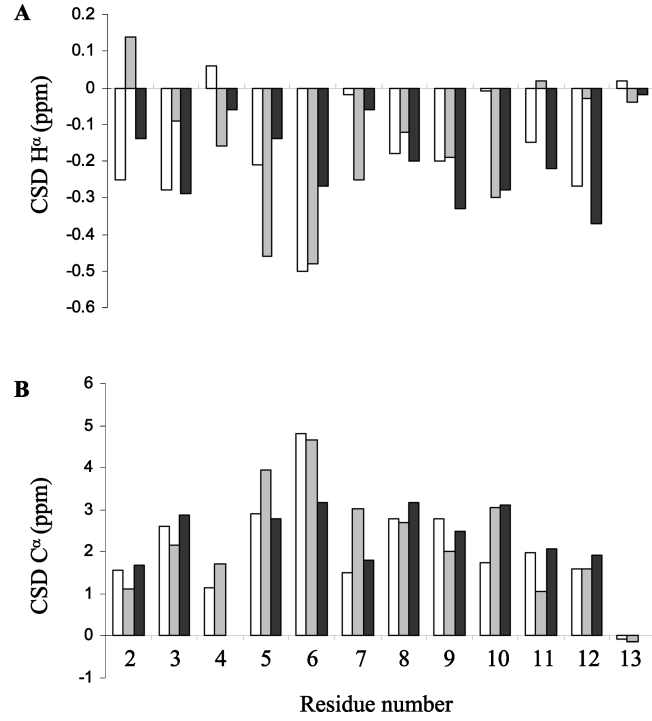

FIGURE 2: Chemical shift deviations (CSDs) of Hα (A) and Cα (B) resonances of temporin-SHa (white bars), -SHb (gray bars), and -SHc (black bars) in micellar SDS.

adopt predominantly helical conformations in micellar SDS (Figure 2). The α-helical conformation was further confirmed by the measurement of $^{3}J_{HN-H\alpha}$ coupling constants smaller than 6 Hz for several residues (Figure 3) and the observation of characteristic NOE correlations throughout the peptide chain, in particular strong sequential $d_{NN}(i,i+1)$ NOEs and typical $d_{\alpha N}(i, i+3)$ and $d_{\alpha\beta}(i,i+3)$ medium-range NOEs (Figure 3). Although temporins are largely helical, the analysis of the CSDs along the sequence reveals different helical propensities of the peptide segments (Figure 2). The N-terminal 1−2 segment of Temp-SHb has the weakest helical propensity. This can be accounted for by a conformational effect of the proline residue in position 3, stabilizing extended conformations of the preceding Leu[2] residue. In contrast, segment 4−6 has a high helical propensity that can be ascribed to a helix initiator conformational effect of Pro[3] on the following residues. The residues in the C-terminal segment of temporins have larger $^{3}J_{HN-H\alpha}$ coupling constants, indicating a greater conformational flexibility in the last turn of the α-helix. Temporins-SH are characterized by the presence of at least one Gly in their sequence, a residue known to have great conformational flexibility and a small propensity for the α_R-helical region in proteins. The Hα resonances of Gly residues have small deviations from random coil values, in comparison with other residues (Figure 3). However medium-range NOEs are observed between residues on either side of Gly residues, indicating that the α-helices are not interrupted by the presence of Gly residues. The residues on either side of Gly adopt mainly helical conformations, as indicated by CSD analysis. The CSDs in position $i+1$ are generally smaller than those in position $i-1$, which may reflect a destabilization of the helix on the C-terminal side of Gly.

Structure of Temporins in Micellar SDS. The solution structures of temporins in 80 mM SDS were calculated by

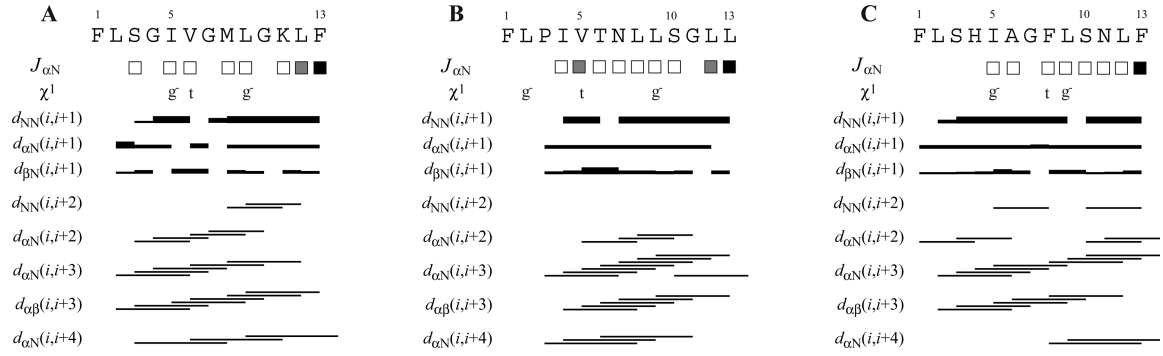

FIGURE 3: Summary of NMR conformational parameters of temporin-SHa (A), -SHb (B), and -SHc (C) in micellar SDS. $^3J_{HN\text{-}H\alpha}$ coupling constants are represented by squares: open square, $J \leq 6$ Hz; gray square, $6 < J < 8$ Hz; filled square, $J \geq 8$ Hz. The χ_1 torsion angles of residues having a major rotamer, based on NOE and/or $^3J_{H\alpha\text{-}H\beta}$ analysis, are indicated: *t*, $\chi_1 \sim 180°$; g^-, $\chi_1 \sim -60°$. The relative intensity of NOE connectivities is indicated by horizontal bars of varying thickness.

restrained molecular dynamics in DYANA and minimized within XPLOR-NIH with CHARMM22 force field to improve the nonbonded term energies and side chain conformations. The NMR families of temporins have good geometrical quality and exhibit few restraint violations (Table S1 in the Supporting Information). The rmsd of all backbone atoms is around 0.7−0.8 Å for the three peptides. The NMR structures of the temporins are shown in Figure 4. In each structure family, segment 3−12 forms a well-defined helix, with backbone rmsds smaller than 0.4 Å. No deformation of the helices is observed around the glycine residues. Residues 1−2 at the N-terminus are more disordered and adopt different conformations in the peptides. In particular, residue 2 in Temp-SHa and -SHc explores mainly the α-helical region of the Ramachandran diagram while it adopts more extended conformations in Temp-SHb. The three-dimensional structures of temporins are stabilized by many i, $i + 3$ and i, $i + 4$ contacts between aliphatic and aromatic side chains. Several side chains of the 4−12 residues adopt a major rotamer around their χ_1 angle as indicated by $^3J_{H\alpha\text{-}H\beta}$ coupling constants and NOE analysis, while others show an equilibrium between *gauche*$^-$ ($\chi_1 \sim -60°$) and *trans* ($\chi_1 \sim 180°$) conformations (Figure 3). These side chains define a large hydrophobic core on one face of the α-helix.

Temporin Orientation in SDS Micelles. The position of temporins relative to the SDS micelle surface was examined using two paramagnetic probes, Mn^{2+} and 5-doxylstearic acid. The spatial proximity of protons with a paramagnetic agent leads to strong enhancements of longitudinal and transversal relaxation. The Mn^{2+} ion is located in the aqueous phase in the vicinity of the anionic headgroups of SDS and is expected to cause selective broadening of residues exposed to the solvent or close to the water−micelle interface. 5-Doxylstearic acid is embedded in the SDS micelle and should cause broadening of residues in the micelle interior but close to the polar heads. For the three temporin peptides, the addition of the doxyl paramagnetic probe caused severe broadening of proton resonances on 1D spectra, in particular of aromatic and methyl resonances, indicating that temporins strongly interact with SDS micelles. The addition of Mn^{2+} also affects proton line widths, indicating that the temporins remain close to the micelle surface. In order to get information for each residue of temporins, the paramagnetic enhancements induced by the two paramagnetic probes were monitored by measuring the residual volumes of HN-Hα and Hα-Hβ cross-peaks on 2D TOCSY spectra (Figure 5). The residues exhibit different sensitivities to the paramagnetic probes depending on their position in the sequence. Interestingly, periodic variations of the residual amplitudes are observed for the three peptides (Figure 5), forming paramagnetic waves (*30*). Indeed, for the three temporin peptides, residues around positions 2, 5, and 9 are strongly affected by 5-doxylstearic acid but are much less sensitive to the Mn^{2+} probe. In contrast, a low sensitivity to the doxyl probe is observed for residues around positions 3, 7, and 11. These periodic variations fit well with the helix amphipathicity, indicating that the use of the two paramagnetic probes enables to discriminate the hydrophobic and polar faces of temporin helices. Furthermore, the variations of paramagnetic enhancements along the sequence suggest that the three temporin peptides should adopt nearly parallel orientations with respect to the micelle surface. For each temporin peptide, residues of the C-terminal 10−13 segment are very sensitive to the Mn^{2+} probe since their HN-Hα correlations completely disappear on the 2D TOCSY spectra. This indicates that the C-terminus is closer to the micelle surface. However, a paramagnetic wave is still observed with 5-doxylstearic acid showing that the C-terminal segment also interacts with the micelle. The analysis of cross-peak attenuations upon addition of Mn^{2+} reveals slight differences between temporins. For Temp-SHa, the central segment 5−9 is less sensitive to the Mn^{2+} probe than the extremities, indicating that it more distant from the surface, in agreement with its hydrophobicity and the absence of polar residues. In Temp-SHb, the least accessible region to the Mn^{2+} probe is shifted toward the N-terminus (segment 2−6). This result can be ascribed to differences in hydropathy, residues 3 and 4 being more hydrophobic and residue 7 more hydrophilic in Temp-SHb. Temp-SHc exhibits an attenuation pattern quite similar to Temp-SHa, although region 7−9 is more sensitive to Mn^{2+}. The observed differences may reflect slight variations in helix orientation and peptide dynamics within the micelle.

Monitoring the Binding of Temporin-SHa and Temporin-SHc to Model Membranes by Differential Scanning Calorimetry. Differential scanning calorimetry was used to study the thermotropic behavior of DMPC and DMPG multilamellar vesicles (MLVs) upon addition of Temp-SHa or Temp-SHc. The peptides were added at different concentrations after liposomes were formed to ensure that they could only interact with the external surface of the MLVs. DMPG

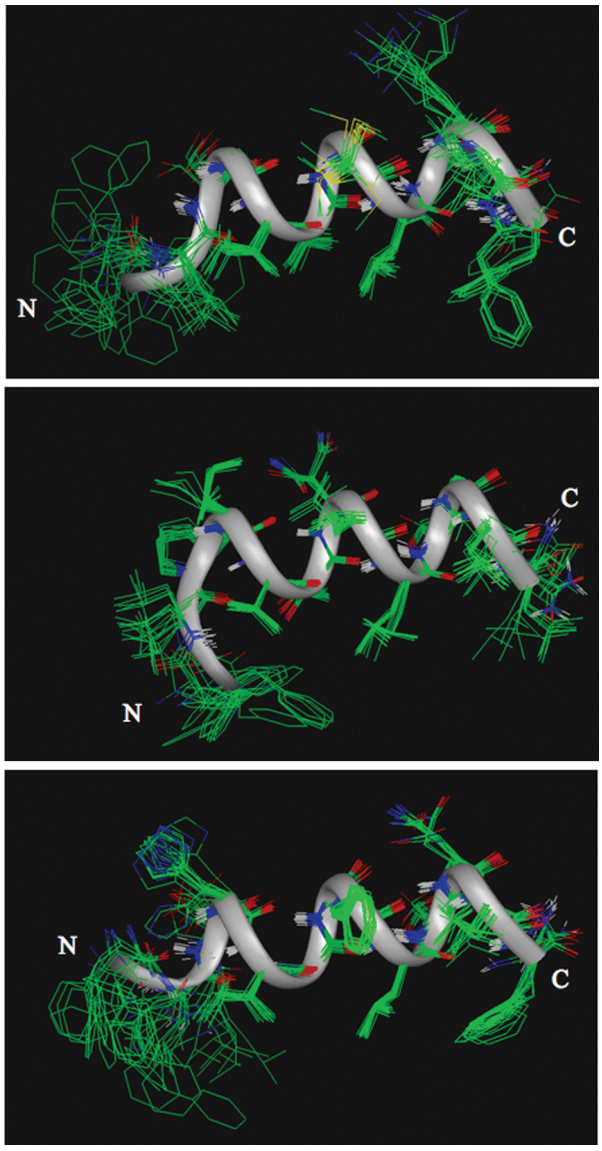

FIGURE 4: NMR structure families of temporin-SHa (A), -SHb (B), and -SHc (C) in micellar SDS. Structures were superimposed by best fitting of backbone N, Cα, and C′ atoms of residues 3−13 to the lowest energy structure. The backbone of the lowest energy structure in each family is shown as a ribbon. Atoms are shown with different colors (amide hydrogen, white; carbon, green; nitrogen, blue; oxygen, red; sulfur, yellow). N and C, N- and C-terminus.

was chosen as a model system for bacterial membranes because they contain substantial (up to 30%) amounts of negatively charged lipids such as phosphatidylglycerol and cardiolipin. DMPC, a zwitterionic phospholipid, was used as a model for mammalian cell membranes. In the absence of peptide, DMPC MLVs exhibit two endothermic events on heating, i.e., a weakly energetic pretransition near 13 °C (conversion of the ordered lamellar gel phase, Lβ', with tilted hydrocarbon chains to the ordered rippled gel phase Pβ') (Figure 6) and a strongly energetic and highly cooperative main transition near 24 °C (conversion of the rippled gel phase to the fluid lamellar liquid-crystalline phase Lα) (Figure 6) (*31, 32*). DSC data from the heating curves reflected essentially the same changes as those from the cooling curves, indicating that thermotropic events were recorded under conditions close to thermodynamic equilibrium. The pretransition is due to interactions between the headgroups of the phospholipids, and increasing the distance between the headgroups eliminates these interactions and causes the pretransition peak to disappear. The main phase transition (chain melting) is mainly due to *trans*−*gauche* interconversion of the acyl chains, which decreases the acyl chain packing of the lipid molecules, increasing fluidity of the membrane. Therefore, the effect of added peptides on the temperature (T_m), enthalpy (ΔH), and cooperativity ($\Delta T_{1/2}$) of the pretransition and the main transition serves as an indicator of the ability of the peptide to interact with lipid headgroups and to perturb the packing of the lipid acyl chains, respectively (*33–35*). The addition of Temp-SHa or Temp-SHc to zwitterionic DMPC vesicles caused only minor effects in the thermotropic phase behavior of the lipids (Figure 6, Table 3). The incorporation of increasing quantities of peptide onto the DMPC bilayers lowers the temperature, the enthalpy, and the cooperativity of the pretransition, abolishing it entirely at a peptide:lipid ratio = 1:100. These results suggest that interaction of the peptides with the lipid headgroups abolishes hydrocarbon chain tilt in the gel phase bilayer, causing the replacement of the Lβ' and Pβ' phases with a disordered Lβ-like phase (*36*). Temp-SHa and Temp-SHc also affect slightly the main lipid phase transition as demonstrated by small increase (Temp-SHc) or decrease (Temp-SHa) in the enthalpy of the main peak with increasing peptide concentration (Figure 6, Table 3). However, the T_m, the half-width, and the shape of the peak change little from those of pure DMPC throughout the peptide concentration range.

Conversely, Temp-SHa and Temp-SHc have considerable, but different perturbing effects on the phase behavior of negatively charged MLVs. In the absence of peptide, DMPG MLVs exhibit a weakly energetic pretransition near 13 °C (conversion of the ordered lamellar gel phase Lβ' to the ordered rippled gel phase Pβ') and a more energetic phase transition near 23 °C (conversion of the rippled gel phase to the fluid lamellar liquid-crystalline phase Lα). The presence of small amounts of Temp-SHa (peptide:lipid ratio = 1:200) strongly reduces the temperature, the enthalpy, and the cooperativity of the pretransition (Figure 6; Table 3). As more peptide is introduced, the pretransition disappears, indicating that there are significant interactions of the peptide with the lipid headgroups. The melting of the acyl chains becomes less cooperative as demonstrated by the decreasing amplitude and increasing half-width of the main transition with increasing peptide concentration. Despite the dramatic change in T_m and cooperativity of the main transition, the ΔH remains close to that of pure DMPG throughout the peptide concentration range, indicating that Temp-SHa decreases the apparent order of the hydrocarbon chains of the liquid-crystalline lipid bilayers. On the other hand, Temp-SHc caused a different perturbing effect than Temp-SHa. At the lowest concentration of peptide:lipid ratio = 1:100, Temp-SHc abolished the pretransition and induced a marked decrease of both T_m and ΔH of the main phase transition, together with an enhanced broadening of the peak and the apparition of a shoulder at the right wing of the main phase transition thermogram (Figure 6). Increasing quantities of the peptide induced a two-component main phase transition consisting of a broad, higher temperature and less cooperative component superimposed over a sharper, lower temperature component. The total enthalpy of the main phase transition decreases rapidly with increasing peptide concentration

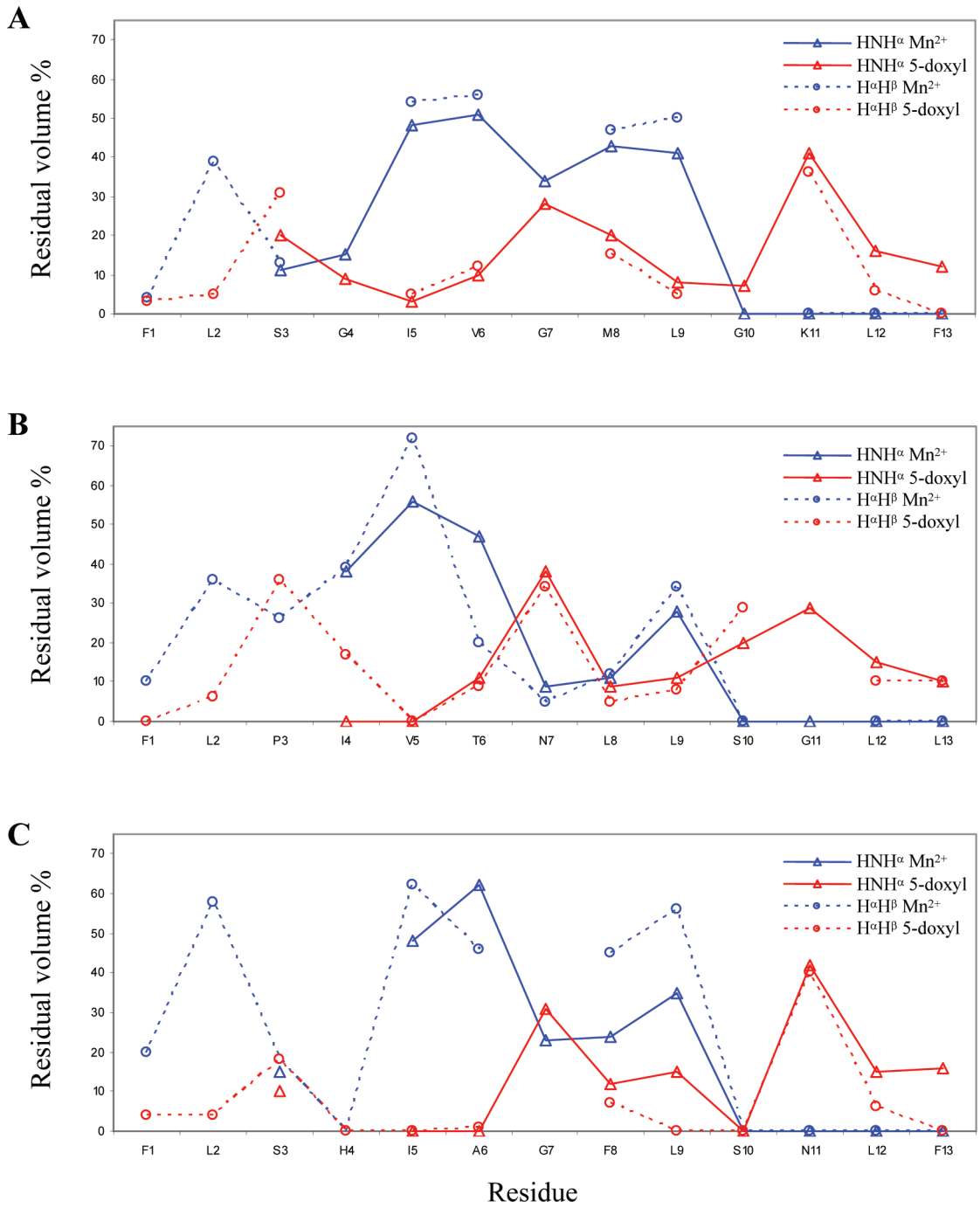

FIGURE 5: Residual volumes of TOCSY cross-peaks of temporin-SHa (A), -SHb (B), and -SHc (C) after addition of paramagnetic probes. The relaxation enhancements induced by Mn^{2+} (0.3 mM) or 5-doxylstearic acid (6.7 mM) are shown in blue and red, respectively. For each residue, the volumes of residual HN-Hα and Hα-Hβ cross-peaks were measured and compared to corresponding correlations on a reference TOCSY recorded in the absence of paramagnetic agent with the same acquisition parameters. For the C-terminal residue of each temporin, the cross-peak between carboxamide protons was analyzed in place of the HN-Hα cross-peak because of the weak intensity of the latter in the reference spectrum.

(Table 3). Using the rationale provided by previous studies (*36, 37*), the sharp and broad components of the DSC endotherms were assigned to the chain melting phase transition of peptide-poor and peptide-rich phospholipid domains, respectively. The decrease in the temperature and cooperativity of the sharp component may be attributable to domain boundary effects arising from the decreasing size of the peptide-poor lipid domain.

Although the peptides were added after liposomes were formed to ensure that they only interact with the external surface of DMPC and DMPG MLVs, high concentrations of Temp-SHa and Temp-SHc abolished the pretransition, suggesting that they altered the phase of the internal MLVs layers. The peptide-induced aggregation and dissociation of DMPG and DMPC MLVs (1 mg/mL) were evaluated by monitoring the turbidity of the lipid suspensions at 436 nm with the same buffer and lipid:peptide molar ratios (1:200, 1:100, and 1:50) used in DSC experiments. Whereas a complete clearance was observed upon the addition of 20 μL of Triton X-100 (10% v/v in water), only a minor and equivalent decrease of the turbidity was observed with Temp-SHa (3%) and Temp-SHc (4%) on DMPG. No changes were

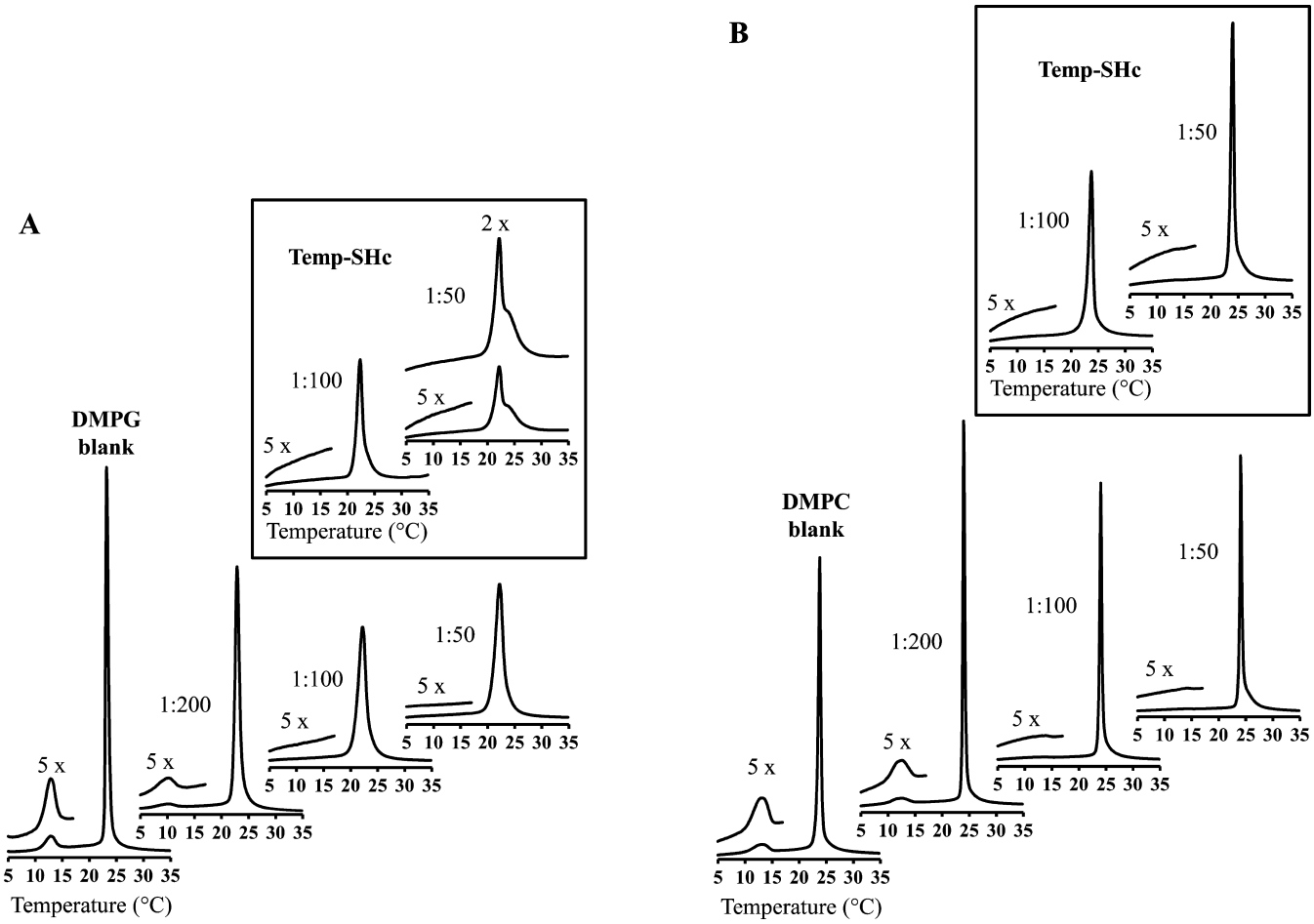

FIGURE 6: DSC heating thermograms illustrating the effect of temporin-SHa and temporin-SHc (insert) on the thermotropic phase behavior of DMPG (A) and DMPC (B) MLVs. The corresponding pretransition regions are shown on a larger scale (5×), and the main transition region has been enlarged (2×) for Temp-SHc/DMPG, 1:50. Scans were acquired at different peptide:lipid molar ratios (temporin-SHa, 1:200, 1:100, and 1:50; temporin-SHc, 1:100 and 1:50).

Table 3: Thermotropic Behavior of DMPC and DMPG Multilamellar Vesicles upon Addition of Temporin-SHa or Temporin-SHc[a]

	pretransition		main transition	
	T_m, °C	ΔH, kcal/mol	T_m, °C	ΔH, kcal/mol
DMPG blank	12.8 ± 0.02	0.9 ± 0.02	23.2 ± 0.02	7.6 ± 0.02
Temp-SHa/DMPG, 1:200	10.2 ± 0.12	0.3 ± 0.00	22.9 ± 0.00	7.8 ± 0.15
Temp-SHa/DMPG, 1:100			22.3 ± 0.00	7.7 ± 0.24
Temp-SHa/DMPG, 1:50			22.3 ± 0.00	7.7 ± 0.29
Temp-SHc/DMPG, 1:100			22.3 ± 0.02	5.12 ± 0.11
Temp-SHc/DMPG, 1:50			22.2 ± 0.02	4.57 ± 0.02
DMPC blank	13.0 ± 0.02	0.9 ± 0.05	23.9 ± 0.00	9.2 ± 0.36
Temp-SHa/DMPC, 1:200	12.1 ± 0.06	0.7 ± 0.02	24.0 ± 0.02	8.8 ± 0.29
Temp-SHa/DMPC, 1:100			24.1 ± 0.00	7.2 ± 0.26
Temp-SHa/DMPC, 1:50			24.1 ± 0.02	7.2 ± 0.18
Temp-SHc/DMPC, 1:100			23.7 ± 0.00	9.3 ± 0.43
Temp-SHc/DMPC, 1:50			24.0 ± 0.02	10.3 ± 0.61

[a] Phase transition temperature (T_m) and total enthalpy for gel to liquid-crystalline transition of DMPG and DMPC MLVs with and without temporin-SHa and temporin-SHc are indicated. Phase transition temperature and total enthalpy were estimated by a peak-fitting procedure using CPCalc software. Values were obtained from six scans and represent the mean ± SEM.

observed for DMPC with both peptides. These results confirm that Temp-SHa and Temp-SHc do not induce aggregation or dissociation of anionic and zwitterionic model membranes. On the other hand, we observed that the thermotropic phase behavior was not completely reproducible for the first few scans presumably because the peptide was progressively gaining access to internal bilayers, so that 5−6 scans were performed before equilibrium was reached. Although no direct physical evidence exists to support this hypothesis, this strongly suggests that temporins may be internalized by exposure to high temperatures and multiple cycling through the gel to liquid phase transition.

Permeabilization of Lipid Vesicles. The membrane-permeabilizing ability of temporin-SHa and temporin-SHc was investigated by measuring the release of the fluorescent marker calcein from zwitterionic (DMPC) or anionic (DMPG) large unilamellar vesicles. As shown in Figure 7, up to 50 μM Temp-SHc was unable to promote the leakage of both types of lipid vesicles in our experimental conditions. In contrast, a substantial difference in the permeabilizing activity of Temp-SHa was observed with an efficiency depending on the vesicle composition. Indeed, Temp-SHa caused the release of approximately 25% of calcein from negatively charged DMPG vesicles and was virtually inactive on neutral DMPC.

DISCUSSION

All proposed models for binding of cationic antimicrobial peptides to bacterial anionic membranes invoke electrostatically driven peptide association at the bilayer surface, followed by hydrophobic adsorption of the peptide at the membrane caused by peptide penetration into the polar

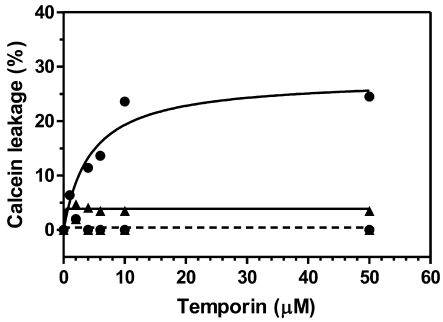

FIGURE 7: Effect of temporin-SHa and temporin-SHc (dotted line) on calcein leakage from DMPG (●) or DMPC (▲) LUVs. Calcein-containing LUVs (400 μM) were incubated 10 min in buffer (10 mM Tris-HCl, 100 mM NaCl, pH 7.4) with increasing concentrations of peptide at 25 °C. The apparent leakage percentage was calculated as described in the Experimental Procedures section. Results are expressed as average values of three independent measurements.

headgroup region only or deeper penetration into the hydrophobic core of the bilayer. An important finding of this work is that Temp-SHa and Temp-SHc exhibit differential capacities to insert into and perturb the anionic bilayer.

The calorimetric data demonstrate that DMPC membranes are only slightly perturbed by Temp-SHa and Temp-SHc in accordance with the low hemolytic activity of the peptides. There were changes in the pretransition that was broadened at low peptide:lipid ratios, slightly shifted toward lower temperatures and which enthalpy was lower. However, it does not indicate either strong disturbance in the membrane or deep peptide penetration in the bilayer (*38*) because the pretransition is very sensitive to the presence of minute amounts of foreign molecules (impurities, ions, drugs, peptides, proteins) even if they interact "electrostatically" and "atmospherically" with the lipid headgroups. The loss of the pretransition can be a consequence of the interaction of peptides with phospholipid headgroups which lead to a spacing between them, thus eliminating the driving force for the formation of a rippled phase. The disappearance of the pretransition was not accompanied by pronounced alterations of the main transition. As the peptide concentration increased, the Lα transition peak was only slightly reduced in amplitude, and $\Delta T_{1/2}$ remains unchanged compared to the untreated DMPC control. This suggests that Temp-SHa and Temp-SHc provoke the disruption of hydrogen bonding at the lipid−water interface by accumulating at the bilayer surface but do not significantly disrupt the acyl chain packing of the DMPC MLVs. The absence of membrane-permeabilization effects of Temp-SHa and Temp-SHc on DMPC LUVs supports this hypothesis. In contrast, DSC results indicated that both peptides interact strongly with anionic DMPG MLVs, not only with the polar region of the phospholipid bilayer, as indicated by changes in the pretransition, but also with the core of the bilayer, as indicated by changes in the main transition. The observation that Temp-SHa and Temp-SHc interact more strongly with anionic DMPG bilayers than with zwitterionic DMPC bilayer is probably due to the more favorable electrostatic and H-bonding interactions between the cationic peptides and the negatively charged surfaces of DMPG bilayers. Accordingly, Temp-SHa permeabilizes negatively charged calcein-loaded DMPG vesicles but not neutral DMPC vesicles. The low leakage efficiency observed (25%) from pure DMPG vesicles could be due to strong electrostatic interactions between cationic residues of Temp-SHa and negatively charged headgroups of DMPG that may anchor the peptide on the membrane surface, restricting its penetration into the bilayer core and thus its lytic activity. The absence of leakage of negatively charged lipid vesicles has been observed for cationic amphipathic peptides such as temporin L, melittin, or the synthetic model peptide KLAL (*9*).

It is evident that Temp-SHa interacts with the anionic bilayer in a different manner from Temp-SHc. Temp-SHa produced a gradual broadening of the main transition peak as a function of peptide concentration. A simple broadening of the main transition without any change in the peak melting temperature would be characteristic of peptides localized in the outer cooperative zone of the bilayer. In the case of Temp-SHa, the main transition peak was both broadened and shifted toward lower temperatures upon binding, indicating fluidification of the membrane and lower packing and van der Waals attraction between lipid molecules as a result of some penetration of the peptide into the hydrophobic domain of the bilayer. The lack of change in ΔH concomitant with the observed T_m lowering and endotherm broadening can be interpreted in terms of peptide forming an approximately ideal solution with the MLVs, consistent with a strong perturbation of the lipid bilayer, in agreement with the strong antibiotic activity of this peptide. Temp-SHa could insert into the lipid bilayer with an orientation either in-plane (parallel) or perpendicular to the surface (*39, 40*). The NMR positioning experiments using paramagnetic probes clearly indicate that temporins-SH bind to SDS micelles with a parallel orientation with respect to the micelle surface. Therefore, an in-plane insertion into the lipid bilayer is very likely.

In contrast, binding of Temp-SHc induced a marked decrease of both T_m and ΔH of the main phase transition, together with an enhanced broadening of the peak and the apparition of a second, broad component at the right wing of the main phase transition thermogram. The appearance of a second component in thermograms of Temp-SHc is a consequence of a nonideal mixing behavior, which creates a nonhomogeneous distribution of the peptide within the membrane. As a result, regions of two coexisting phases, one phase rich in peptide (higher temperature) and the other lipid-rich (lower temperature), could be formed. This gradual phase segregation between peptide-poor and peptide-rich domains may eventually lead to membrane disruption. According to the classification of Papahadjopoulos et al. and McElhaney et al. (*41, 42*), Temp-SHc would thus be considered as a type II peptide which most likely resides at the hydrocarbon core−water interface of the lipid bilayer, interacting with the polar headgroups and glycerol backbone region of the phospholipids and the region of the lipid acyl chain near the bilayer surface only.

The three temporin peptides exhibit high helical propensities in structure-promoting solvents such as TFE or micellar SDS, as inferred by CD analysis. A greater stabilization of helices is observed in SDS, suggesting different driving forces for α-helical formation, as already observed for other antimicrobial peptides (*43*). The NMR conformational studies were carried out in micellar SDS, which is considered as a better membrane-mimetic system than TFE. The determination of the three-dimensional structure of these peptides bound to anionic micelles of SDS allowed us to evaluate

whether the great differences observed between their effects on anionic membranes could be rationalized in terms of degree of structure formation, amphipathicity, and/or hydrophobicity and peptide location in the membrane-mimetic system. The NMR study shows that temporin peptides adopt well-defined α-helices with a large hydrophobic face in the presence of SDS micelles. The differences in local helical propensities can be rationalized in terms of sequence variation, such as the conformational effect of proline in Temp-SHb. The peptides differ by the absence or presence of a cationic side chain. Although Temp-SHb lacks a cationic side chain, it has a helical propensity similar to Temp-SHa and -SHc. This indicates that the helical stabilization of temporins in anionic micelles is primarily driven by hydrophobic interactions rather than electrostatic interactions. Temp-SHa and -SHc have a cationic His or Lys side chain in the first or last turn of the α-helices, respectively. The His imidazole group was shown to be protonated in the conditions of the NMR study, on the basis of its $H^{\epsilon 1}$ chemical shift. The position of the cationic side chain either in the N-terminal part or in the C-terminal part has no effect on the helix stabilization of temporins. A characteristic of these temporins is the presence of Gly residues in the helix. In particular, Temp-SHa has three Gly residues in positions 4, 7, and 10 but still adopts a well-defined helix. All of the Gly residues are located on the polar face of the helix. Therefore, the presence of Gly does not destabilize the hydrophobic interactions on the apolar face of the helix. The amphipathic character of temporins-SH is highlighted on a Shiffer−Edmundson helical wheel representation (*44*), with two well-separated clusters of hydrophobic and hydrophilic/basic residues located on opposing sides of the helical wheel (Figure 1). Whereas the polar face of the Temp-SHc helix subtends a radial angle of 180° perpendicular to the long axis, that of Temp-SHa is much smaller (∼100°), with only two polar side chains.

The location of temporins with respect to the micelle was analyzed by monitoring relaxation enhancements induced by a water-soluble or a lipophilic paramagnetic probe. The peptides do not penetrate deeply in the micelle core but are located near the micelle surface, since they are sensitive to both Mn^{2+} and 5-doxylstearic acid probes. The observed relaxation waves clearly indicate that the peptides adopt nearly parallel orientations with respect to the micelle surface. The C-terminal part of temporins was found to be more sensitive to the Mn^{2+} probe, suggesting that it is pointing toward the micelle surface. However, the hydrophobic residues in positions 12 and 13 are also sensitive to the doxyl probe, indicating that their side chains are anchored into the micelle. The slight modifications in paramagnetic attenuations observed between temporins could be ascribed to subtle changes in helix tilt and depth of immersion. Additionally, the time averaging of paramagnetic relaxation enhancement makes it sensitive to factors such as peptide conformational flexibility or peptide motions within the micelle. Accordingly, the conformational heterogeneity in the last turn of the α-helix might explain the higher sensitivity of the 10−13 segment to the Mn^{2+} probe in the three temporins. The C-terminal part could interconvert between α-helical and unfolded conformations that would position the residues at the water−micelle interface. In contrast, the central parts of temporin helices are less subject to conformational heterogeneity so that their paramagnetic enhancements depend mainly on the depth of immersion and on dynamic equilibria of the peptides within the micelle or between the micelle interior and the micelle−water interface. Overall, the three temporin peptides exhibit the same order of sensitivity toward both paramagnetic probes, suggesting that their average immersion depths are close. Therefore, the slight differences in the attenuation patterns observed between temporins likely reflect the amplitude of peptide translational motions inward or outward. We observed that the presence of a polar side chain in the central segment of temporins is associated with an increased sensitivity to Mn^{2+} probe, as observed for the His^4 residue in Temp-SHc or Asn^7 residue in Temp-SHb, whereas the sensitivity to the doxyl probe is not decreased. A possible explanation is that the average immersion depth remains unchanged while the amplitude of translational motions enables the peptide to get closer to the surface. Since Temp-SHa does not have any polar side chain in positions 4, 7, and 10, it is less prone to get close to the surface, explaining the low attenuations in the 5−9 segment by Mn^{2+}.

Temp-SHa and Temp-SHc have highly similar membrane-bound helical structures, plus identical mean hydrophobic moments, mean hydrophobicities (Table 1), and amphipathicities. Both peptides have numerous Leu and Phe residues, which are known to serve as membrane anchors in transmembrane helices (*45*), and a similar potential to act as amphipathic in-plane membrane anchors (*46*). It is thus likely that the differences in membrane-perturbing properties of the two peptides may reflect the peculiar properties of the Lys residue near the C-terminus of Temp-SHa (instead of a His residue near the N-terminus in Temp-SHc), as well as subtle differences in the amino acid composition of the polar face of the peptides. An obvious explanation is that long-range Coulombic attractions between the peptides and the negatively charged headgroups of the DMPG MLVs are much weaker in the case of Temp-SHc. The His side chain has a pK_a value close to 6.5 when in an unstructured polypeptide chain, thus being positively charged at acidic pH and only weakly charged at pH ≥7. One would therefore expect that higher concentrations of Temp-SHc are needed to bind to anionic membranes and kill bacteria in functional assays at physiological pH. This is the case for several naturally occurring and synthetic polyhistidine-rich antimicrobial peptides, such as clavinins (*47*), histatins (*48*), and LAH4 (*49*). Note, however, that the ionization state of the His residue can be modulated by hydrophobic, electrostatic, and polar interactions with anionic surfaces. For instance, a large shift of pK_a of the His residue to a much higher value is expected if His acts as a hydrogen bond donor to form a H-bond with the anionic headgroups of negatively charged bilayers via its $N^{\delta 1}H^+$ or $N^{\epsilon 2}H^+$ groups.

Although Temp-SHc-membrane association at pH 7.5 must be reduced when compared with Temp-SHa, this phenomenon does not provide a basis for the differential capacities of these peptides to insert into and to perturb the anionic bilayers. An additional explanation invokes differences between polar surfaces of the two peptides. As already mentioned, the polar face of Temp-SHa is rather small, being constituted of only two polar side chains (Ser and Lys). The three Gly residues may also provide conformational adaptability to the peptide chain, thereby facilitating insertion into the lipid bilayer. However, a greater conformational flex-

ibility around the Gly residues was not observed in SDS micelles. In addition, the polar face of Temp-SHc contains two Ser residues and one Asn residue, which prefer to be localized at the level of the polar and negatively charged groups of the bilayer surface, where favorable electrostatic and hydrogen-bonding interactions are maximized. These interactions would additionally impede peptide insertion. This phenomenon, which does not bear out the obvious role of the overall peptide net charge, may explain why Temp-SHa and Temp-SHc interact in different ways with anionic membrane models at pH 7.5 and the reduced efficacy of Temp-SHc against bacteria.

Although the results presented here provide insights to the understanding of temporin−lipid interactions, they show that our present knowledge of the mechanism of membrane permeabilization and disruption of bacterial cells is not sufficient to safely predict antimicrobial potencies and selectivities of this class of peptides by biophysical approaches involving simple model membranes. In addition, an intriguing observation is that Temp-SHc is as potent as Temp-SHa to kill yeasts despite the fact that the plasma membrane of *Candida* species contains a large proportion of negatively charged phospholipids, namely, phosphatidic acid and phosphatidylglycerol. Thus, the possibility that these peptides act against yeasts via other mechanisms, i.e., inhibition of metabolic functions, binding to DNA, or altering the function of membrane-bound multienzyme complexes such as electron transport chains, cannot be excluded.

ACKNOWLEDGMENT

We thank Drs. L. Lajavardi and J. Nicolas for help in calcein leakage experiments.

SUPPORTING INFORMATION AVAILABLE

Table S1, structural statistics for the NMR families of temporins-SH in micellar SDS. This material is available free of charge via the Internet at http://pubs.acs.org.

REFERENCES

1. Simmaco, M., Mignogna, G., Canofeni, S., Miele, R., Mangoni, M. L., and Barra, D. (1996) Temporins, antimicrobial peptides from the European red frog Rana temporaria. *Eur. J. Biochem. 242*, 788–792.
2. Conlon, J. M., Kolodziejek, J., and Nowotny, N. (2004) Antimicrobial peptides from ranid frogs: taxonomic and phylogenetic markers and a potential source of new therapeutic agents. *Biochim. Biophys. Acta 1696*, 1–14.
3. Conlon J. M. (2006) The Temporins, in *Handbook of Biologically Active Peptides* (Kastin, A. J., Ed.) pp 305−309, Elsevier, San Diego, CA.
4. Mangoni, M. L. (2006) Temporins, anti-infective peptides with expanding properties. *Cell. Mol. Life Sci. 63*, 1060–1069.
5. Mangoni, M. L., Rinaldi, A. C., Di Giulio, A., Mignogna, G., Bozzi, A., Barra, D., and Simmaco, M. (2000) Structure-function relationships of temporins, small antimicrobial peptides from amphibian skin. *Eur. J. Biochem. 267*, 1447–1454.
6. Wade, D., Silberring, J., Soliymani, R., Heikkinen, S., Kilpeläinen, I., Lankinen, H., and Kuusela, P. (2000) Antibacterial activities of temporin A analogs. *FEBS Lett. 479*, 6–9.
7. Giacometti, A., Cirioni, O., Kamysz, W., D'Amato, G., Silvestri, C., Del Prete, M. S., Licci, A., Lukasiak, J., and Scalise, G. (2005) In vitro activity and killing effect of temporin A on nosocomial isolates of Enterococcus faecalis and interactions with clinically used antibiotics. *J. Antimicrob. Chemother. 55*, 272–274.
8. Mangoni, M. L., Saugar, J. M., Dellisanti, M., Barra, D., Simmaco, M., and Rivas, L. (2005) Temporins, small antimicrobial peptides with leishmanicidal activity. *J. Biol. Chem. 280*, 984–990.
9. Rinaldi, A. C., Mangoni, M. L., Rufo, A., Luzi, C., Barra, D., Zhao, H., Kinnunen, P. K., Bozzi, A., Di Giulio, A., and Simmaco, M. (2002) Temporin L: antimicrobial, haemolytic and cytotoxic activities, and effects on membrane permeabilization in lipid vesicles. *Biochem. J. 368*, 91–100.
10. Urbán, E., Nagy, E., Pál, T., Sonnevend, A., and Conlon, J. M. (2007) Activities of four frog skin-derived antimicrobial peptides (temporin-1DRa, temporin-1Va and the melittin-related peptides AR-23 and RV-23) against anaerobic bacteria. *Int. J. Antimicrob. Agents 29*, 317–321.
11. Carotenuto, A., Malfi, S., Saviello, M. R., Campiglia, P., Gomez-Monterrey, I., Mangoni, M. L., Gaddi, L. M., Novellino, E., and Grieco, P. (2008) A different molecular mechanism underlying antimicrobial and hemolytic actions of temporins A and L. *J. Med. Chem. 51*, 2354–2362.
12. Matsuzaki, K., Murase, O., Fujii, N., and Milyjmak, K. (1996) An antimicrobial peptide, magainin 2, induced rapid flip-flop of phospholipids coupled with pore formation and peptide translocation. *Biochemistry 35*, 11361–11368.
13. Shai, Y. (1999) Mechanism of the binding, insertion and destabilization of phospholipid bilayer membranes by α-helical antimicrobial and cell non-selective membrane-lytic peptides. *Biochim. Biophys. Acta 1462*, 55–70.
14. Bechinger, B., and Lohner, K. (2006) Detergent-like actions of linear amphipathic cationic antimicrobial peptides. *Biochim. Biophys. Acta 1758*, 1529–1539.
15. Abbassi, F., Oury, B., Blasco, T., Sereno, D., Bolbach, G., Nicolas, P., Hani, K., Amiche, M., and Ladram, A. (2008) Isolation, characterization and molecular cloning of new temporins from the skin of the North African ranid Pelophylax saharica, *Peptides 29*, 1526−1533.
16. Conlon, J. M. (2008) Reflections on a systematic nomenclature for antimicrobial peptides from the skins of frogs of the family Ranidae, Peptides (in press).
17. Vanhoye, D., Bruston, F., El Amri, S., Ladram, A., Amiche, M., and Nicolas, P. (2004) Membrane association, electrostatic sequestration, and cytotoxicity of Gly-Leu-rich peptide orthologs with differing functions. *Biochemistry 43*, 8391–8409.
18. Lequin, O., Ladram, A., Chabbert, L., Bruston, F., Convert, O., Vanhoye, D., Chassaing, G., Nicolas, P., and Amiche, M. (2006) Dermaseptin S9, an α-helical antimicrobial peptide with a hydrophobic core and cationic termini. *Biochemistry 45*, 468–480.
19. Rucker, S. P., and Shaka, A. J. (1989) Broadband homonuclear cross polarization in 2D NMR using DIPSI-2. *Mol. Phys. 58*, 509–517.
20. Sklenar, V., Piotto, M., Leppik, R., and Saudek, V. (1993) Gradient-tailored water suppression for proton-nitrogen-15 HSQC experiments optimized to retain full sensitivity. *J. Magn. Reson. A 102*, 241–245.
21. Lippens, G., Dhalluin, C., and Wieruszeski, J. M. (1995) Use of a water flip-back pulse in the homonuclear NOESY experiment. *J. Biomol. NMR 5*, 327–331.
22. Dhalluin, C., Wieruszeski, J. M., and Lippens, G. (1996) An improved homonuclear TOCSY experiment with minimal water saturation. *J. Magn. Reson. B 111*, 168–170.
23. Schleucher, J., Schwendinger, M., Sattler, M., Schmidt, P., Schedletzky, O., Glaser, S. J., Sorensen, O. W., and Griesinger, C. (1994) A general enhancement scheme in heteronuclear multidimensional NMR employing pulsed field gradients. *J. Biomol. NMR 4*, 301–306.
24. Bartels, C., Xia, T. H., Billeter, M., Güntert, P., and Wüthrich, K. (1995) The program XEASY for computer-supported NMR spectral analysis of biological macromolecules. *J. Biomol. NMR 6*, 1–10.
25. Szyperski, T., Güntert, P., Otting, G., and Wüthrich, K. (1992) Determination of scalar coupling constants by inverse Fourier transformation of in-phase multiplets. *J. Magn. Reson. 99*, 552–560.
26. Wishart, D. S., Bigam, C. G., Holm, A., Hodges, R. S., and Sykes, B. D. (1995) ^{1}H, ^{13}C and ^{15}N random coil NMR chemical shifts of the common amino acids. I. Investigations of nearest-neighbor effects. *J. Biomol. NMR 5*, 67–81.
27. Güntert, P., Mumenthaler, C., and Wüthrich, K. (1997) Torsion angle dynamics for NMR structure calculation with the new program DYANA. *J. Mol. Biol. 273*, 283–298.
28. Schwieters, C. D., Kuszewski, J. J., Tjandra, N., and Clore, M. G. (2003) The Xplor-NIH NMR molecular structure determination package. *J. Magn. Reson. 160*, 65–73.
29. Laskowski, R. A., Rullmannn, J. A., MacArthur, M. W., Kaptein, R., and Thornton, J. M. (1996) AQUA and PROCHECK-NMR:

programs for checking the quality of protein structures solved by NMR. *J. Biomol. NMR 8*, 477–486.
30. Respondek, M., Madl, T., Göbl, C., Golser, R., and Zangger, K. (2007) Mapping the orientation of helices in micelle-bound peptides by paramagnetic relaxation waves. *J. Am. Chem. Soc. 129*, 5258–5234.
31. Lewis, R. N. A. H., Mak, N., and McElhaney, R. N. (1987) A differential scanning calorimetric study of the thermotropic phase behavior of model membranes composed of phosphatidylcholines containing linear saturated fatty acyl chains. *Biochemistry 26*, 6118–6126.
32. Zhang, Y.-P., Lewis, R. N. A. H., and McElhaney, R. N. (1997) Calorimetric and spectroscopic studies of the thermotropic phase behavior of the n-saturated 1,2-diacylphosphatidylglycerols. *Biophys. J. 72*, 779–793.
33. McElhaney, R. N. (1986) Differential scanning calorimetric studies of lipid-protein interactions in model membrane systems. *Biochim. Biophys. Acta 864*, 361–421.
34. Lohner, K., and Prenner, E. J. (1999) Differential scanning calorimetry and X-ray diffraction studies of the specificity of the interaction of antimicrobial peptides with membrane-mimetic systems. *Biochim. Biophys. Acta 1462*, 141–156.
35. Henzler-Wildman, K. A., Martinez, G. V., Brown, M. F., and Ramamoorthy, A. (2004) Perturbation of the hydrophobic core of lipid bilayers by the human antimicrobial peptide LL-37. *Biochemistry 43*, 8459–8469.
36. Zhang, Y. P., Lewis, R. N., Hodge, R. S., and McElhaney, R. N. (1995) Peptide models of helical hydrophobic transmembrane segments of membrane proteins. 2. Differential scanning calorimetric and FTIR spectroscopic studies of the interaction of Ac-K2-(LA)12-K2-amide with phosphatidylcholine bilayers. *Biochemistry 34*, 2362–2371.
37. Seto, G. W. J., Marwaha, S., Kobewka, D. M., Lewis, R. N., Separovic, F., and McElhaney, R. N. (2007) Interactions of the Australian tree frog antimicrobial peptides aurein 1.2, citropin 1.1 and maculatin 1.1 with lipid model membranes: differential scanning calorimetric and Fourier transform infrared spectroscopic studies. *Biochim. Biophys. Acta 1768*, 2787–2800.
38. Suezaki, Y., Tatara, T., Kaminoh, Y., Kamaya, H., and Ueda, I. (1990) A solid-solution theory of anesthetic interaction with lipid membranes: temperature span of the main phase transition. *Biochim. Biophys. Acta 1029*, 143–148.
39. Bae, S. J., Kitamura, S., Herbette, L. G., and Sturtevant, J. M. (1989) The effects of calcium channel blocking drugs on the thermotropic behavior of dimyristoylphosphatidylcholine. *Chem. Phys. Lipids 51*, 1–7.
40. Fresta, M., Ricci, M., Rossi, C., Furneri, P. M., and Puglisi, G. (2000) Antimicrobial nonapeptide leucinostatin A-dependent effects on the physical properties of phospholipid model membranes. *J. Colloid Interface Sci. 226*, 22–30.
41. Papahadjopoulos, D., Moscarello, M., Eylar, E. H., and Isac, T. (1975) Effects of proteins on thermotropic phase transitions of phospholipid membranes. *Biochim. Biophys. Acta 401*, 317–335.
42. McElhaney, R. N. (1982) The use of differential scanning calorimetry and differential thermal analysis in studies of model and biological membranes. *Chem. Phys. Lipids 30*, 229–259.
43. Lequin, O., Bruston, F., Convert, O., Chassaing, G., and Nicolas, P. (2003) Helical structure of Dermaseptin B2 in a membrane-mimetic environment. *Biochemistry 42*, 10311–10323.
44. Schiffer, M., and Edmundson, A. B. (1967) Use of helical wheels to represent the structures of proteins and to identify segments with helical potential. *Biophys. J. 7*, 121–135.
45. Meijer, A. B., Spruijt, R. B., Wolfs, C. J., and Hemminga, M. A. (2001) Membrane-anchoring interactions of M13 major coat protein. *Biochemistry 40*, 8815–8820.
46. Sapay, N., Guermeur, Y., and Deléage, G. (2006) Prediction of amphipathic in-plane membrane anchors in monotopic proteins using a SVM classifier, BMC. *Bioinformatics 7*, 255.
47. Lee, I. H., Zhao, C., Cho, Y., Harwig, S. S., Cooper, E. L., and Lehrer, R. I. (1997) Clavanins, α-helical antimicrobial peptides from tunicate hemocytes. *FEBS Lett. 400*, 158–162.
48. Raj, P. A., Soni, S. D., and Levine, M. J. (1994) Membrane-induced helical conformation of an active candidacidal fragment of salivary histatins. *J. Biol. Chem. 269*, 9610–9619.
49. Bechinger, B. (1996) Towards membrane protein design: pH-sensitive topology of histidine-containing polypeptides. *J. Mol. Biol. 263*, 768–775.

BI8006884